Experimental Demonstration of Electron Longitudinal-Phase-Space Linearization by Shaping the Photoinjector Laser Pulse

G. Penco,[1,*] M. Danailov,[1] A. Demidovich,[1] E. Allaria,[1] G. De Ninno,[1,2] S. Di Mitri,[1] W. M. Fawley,[1,3] E. Ferrari,[1,4] L. Giannessi,[1,5] and M. Trovó[1]

[1]*Elettra-Sincrotrone Trieste S.C.p.A., S.S. 14-km 163.5 in AREA Science Park 34149 Basovizza, Trieste, Italy*
[2]*University of Nova Gorica, 5000 Nova Gorica, Slovenia*
[3]*SLAC National Accelerator Laboratory, Menlo Park, California 94025, USA*
[4]*Dipartimento di Fisica, Università degli Studi di Trieste, Piazzale Europa 1, 34127 Trieste, Italy*
[5]*Enea, via Enrico Fermi 45, 00044 Frascati, Roma, Italy*

(Received 11 September 2013; published 31 January 2014)

Control of the electron-beam longitudinal-phase-space distribution is of crucial importance in a number of accelerator applications, such as linac-driven free-electron lasers, colliders and energy recovery linacs. Some longitudinal-phase-space features produced by nonlinear electron beam self- fields, such as a quadratic energy chirp introduced by geometric longitudinal wakefields in radio-frequency (rf) accelerator structures, cannot be compensated by ordinary tuning of the linac rf phases nor corrected by a single high harmonic accelerating cavity. In this Letter we report an experimental demonstration of the removal of the quadratic energy chirp by properly shaping the electron beam current at the photoinjector. Specifically, a longitudinal ramp in the current distribution at the cathode linearizes the longitudinal wakefields in the downstream linac, resulting in a flat electron current and energy distribution. We present longitudinal-phase-space measurements in this novel configuration compared to those typically obtained without longitudinal current shaping at the FERMI linac.

DOI: 10.1103/PhysRevLett.112.044801 PACS numbers: 41.85.Ct, 29.20.Ej, 29.27.Bd, 41.60.Cr

High-energy electron accelerators are advanced tools for research in many scientific fields, including elementary particle physics, nuclear physics, nuclear medicine, synchrotron light sources and free-electron lasers (FELs). As such, they require state of the art control of the accelerator output beam properties, as energy, peak current and/or the detailed shape of the electron beam transverse and longitudinal-phase-space (LPS). The accurate control of the latter turns out to be particularly important in a number of different contexts, such as colliders [1,2], energy recovery linacs [3,4] and short wavelength FELs that today are revolutionizing science at ultrasmall and ultrafast scales [5].

Resonant FEL emission occurs at a wavelength $\lambda_R = (\lambda_u/2\gamma^2)(1 + K^2)$, where $K = eB_u\lambda_u/(2\pi m_e c)$ is the normalized undulator strength, λ_u and B_u are, respectively, the undulator period and peak magnetic field, and $\gamma m_e c^2$ is the electron energy. For a high-gain FEL [6–8], variation of γ along the bunch can lead to an unwanted chirp and/or to spectral broadening. In the following, we focus on the high-gain harmonic generation (HGHG) scheme [9], where an external seed laser temporally overlaps and coherently modulates the electron beam energy in a short undulator (the "modulator"). The beam then passes through a chromatic dispersive section where the energy modulation is converted into a density modulation with a significant spectral content at high harmonics of the seed laser wavelength. The microbunched electron beam then enters a subsequent undulator chain (the "radiator") tuned to a high harmonic of the seed wavelength, and consequently emits coherent radiation that is strongly amplified as the beam passes through the undulators. If the electron beam and seed pulse properties are both temporally homogeneous, the output radiation bandwidth can approach the Fourier transform limit. However, the combination of the large momentum compaction R_{56} of the dispersive section, together with a beam energy chirp, leads to a deterministic compression of the seed-induced modulation, shifting the output FEL wavelength. In fact, while a linear energy chirp produces a constant wavelength shift, a *quadratic* chirp can seriously increase the bandwidth far beyond the Fourier transform limit.

The problem of quadratic-chirp bandwidth degradation was identified early in the design of the HGHG-based FERMI [10,11] and considered as one of the main factors limiting the spectral purity of seeded-FEL sources in general [12–15]. Experimentally, chirp-induced wavelength shifts have been observed for FERMI [7,16]. Although the effect could be compensated by a reverse chirp of the seed laser, by far the most attractive solution is to eliminate as much as possible energy chirps and current variations in the electron beam before it enters the modulator. In this Letter we present the first successful experimental demonstration of LPS linearization obtained at the FERMI linac by shaping the electron bunch density at the injector.

Several elements contribute to the final electron-beam linear and quadratic energy chirp. First, rf accelerating

sections provide a negative quadratic chirp, so that the electron energy E is increased according to $E(t) = \Sigma_i eV_i \cos(\omega_{rf} t + \phi_i)$, where t is the bunch internal temporal coordinate, ω_{rf} is the rf frequency, and V_i and ϕ_i are the rf voltage and phase of the ith section. Second, in a bunch-compressor magnetic-chicane, adopted to shorten the electron bunch, a particle with a fractional energy deviation $\delta = \delta E/E_0$ will be temporally shifted by an amount: $\Delta t = (R_{56}/c)\delta - (3R_{56}/2c)\delta^2 + \mathcal{O}(\delta^3)$ [17]. The momentum compaction R_{56} of a four-dipole chicane is negative and provides a negative curvature to the electrons LPS. A high-harmonic rf cavity is usually implemented [18,19] to compensate the nonlinearity of both the chicane and the upstream rf curvature, providing the necessary positive quadratic chirp to the electrons LPS and guaranteeing a linear longitudinal compression. Nonetheless, the harmonic voltage and phase cannot be chosen so as to further compensate the LPS distortions occurring in the downstream linac, without losing the linearization of the compression process and thus the flatness of the final bunch current profile.

An important downstream LPS distortion comes from the geometric longitudinal wakefields generated in rf sections. According to [20], the wakefield potential is $W(s) = -\int_0^\infty w(s')\rho(s-s')ds'$, where $\rho(s)$ is the longitudinal charge distribution and $w(s)$ is the wake function, i.e., the point charge voltage loss [21], generally written as $w(s) = AZ_0 c/\pi a^2 \exp(-\sqrt{s/s_0})$. Here A, s_0 are fitting parameters that depend upon the cavity geometry, Z_0 is the vacuum impedance (377 Ω), and a is the accelerating structure inner radius. For complex geometries, such as the backward-traveling wave (BTW) structures installed in the FERMI linac [22], $w(s)$ is much larger than in the usual traveling wave SLAC-type structures, because of the smaller inner radius a of the former. This is typically the case also for higher rf frequency structures, such as the X-band linac of the CLIC project [23] and the C-band linacs in the Swiss-XFEL (PSI) [24] and SACLA [25]. The sign of curvature in the LPS due to the wakes is positive in our convention and opposite to those induced by the main rf curvature and the bunch compressor.

One possibility to reduce this positive wake-induced curvature exploits two-stage compression, using the second order dispersion term $(-(3R_{56}/2c))$ of the second chicane to provide the necessary negative curvature. However, cancellation of the final wake-induced quadratic chirp may require a very large R_{56} in the second chicane. This enhances both coherent synchrotron radiation (CSR) emission [26] and microbunching instability growth [27] that can degrade both the transverse and the longitudinal beam emittance.

It is therefore necessary to find another free parameter to compensate the wake nonlinearity in order to generate an output electron-bunch homogeneous in current and energy. This issue was theoretically addressed in Ref. [28], where,

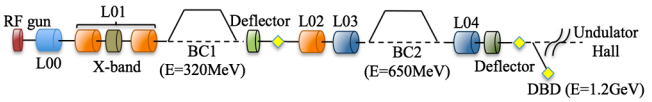

FIG. 1 (color online). FERMI linac layout including the rf photocathode gun, linac $L00$, $L01$, $L02$, $L03$, and $L04$, the X-band cavity and the two bunch compressors (BC1 and BC2). rf defecting cavities for diagnosing time-resolved parameters are installed after BC1 and at the linac end.

starting from the assumption that the output bunch configuration is largely predetermined by the input bunch configuration, temporal shaping of the longitudinal current density at the injector was proposed as the possible additional free parameter. Numerical simulations showed that a linearly ramped current distribution at the injector exit could linearize the wakes generated in the downstream linac sections. One method to generate such a current profile consists of shaping the temporal photoinjector laser (PIL) intensity. We report here an experimental demonstration that a properly shaped beam current profile, effectively compensates the nonlinearity of the downstream wakes and linearizes the LPS at the linac end, validating the theoretical study published in [28]. The experiment was performed at the FERMI facility, whose layout is reported in Fig. 1.

The FERMI electron beam is generated in a 1.6-cell rf photocathode gun [29], accelerated first to ≈ 100 MeV by a two-section linac ($L00$), then to ≈ 320 MeV by a four-section linac (L01). The rf phases of the latter are set off-crest to impose the time-energy correlation needed for the compression in the following magnetic chicane (BC1). An X-band cavity, resonant at the fourth harmonic of the main rf system and located between L01 and BC1, linearizes the compression. After BC1, two linacs (L02 and L03) accelerate the beam to ≈ 650 MeV; optionally these can be set off-crest to further compress the beam in a second magnetic chicane (BC2) [30]. Finally, L04 accelerates the beam to an output energy of 1.2 to 1.5 GeV. Radio frequency deflecting cavities are located after BC1 for studying the post-chicane time-resolved beam parameters, and, in

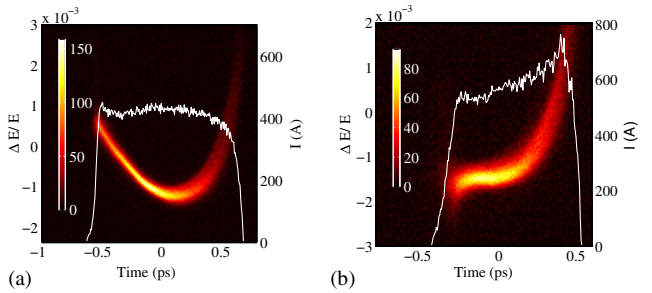

FIG. 2 (color online). LPS measured at the end of the linac (at about 1.2 GeV) in the flat-top bunch, single stage compression scheme usually adopted in the FERMI linac (a) and in the double-stage compression scheme (b). The right axis refers to the current profile (white line). The bunch head lies to the left.

TABLE I. Coefficients of the third-order polynomial fitting of the LPS measured under single-stage and double-stage compression schemes.

	χ_1[MeV/ps]	χ_2[MeV/ps^2]	χ_3[MeV/ps^3]
Only BC1	−0.04	21	50
BC1 and BC2	0.56	10	67

combination with an energy spectrometer in a diagnostic beam dump (DBD) [31], also at the linac end. There the beam, vertically stretched by the deflector and horizontally energy-dispersed by the DBD dipole, is intercepted by a YAG screen that permits measurement of the output LPS.

The L03 and L04 linacs consist of BTW sections with strong wakefields that affect the electron beam LPS. Figure 2 shows the typical LPS measured in two separate cases. The first is the nominal operation condition that consists of generating a flat-top, 500 pC bunch at the injector and compressing it with BC1 only, to obtain a current of ~400–500 A [Fig. 2(a)]. In the second case [see Fig. 2(b)], the BC2 chicane is also activated and set to an angle close to its maximum value ($R_{56}^{BC2} = -40$ mm). The electron LPS measured in these two cases is fitted with a third order polynomial, $E(t) = E_0 + \chi_1 t_1 + \frac{1}{2}\chi_2 t_2^2 + \frac{1}{6}\chi_3 t_3^3$. The results are summarized in Table I.

In both cases, the LPS shows strong energy nonlinearities that significantly affect FEL performance [16]. In single-stage compression operation the current profile is nearly constant but the energy curvature (χ_2) is much larger than the design specification (0.8 MeV/ps^2 [11]). Despite a reduction by a factor 2 in the double-stage compression case, the χ_2 term remains too large. Moreover, operating with both bunch compressors increases the beam incoherent energy spread by about 20%, as predicted by [32,33], leading to an observed deterioration of the FEL performance [34].

More significant progress in linearizing the final LPS was obtained by shaping the bunch density profile at the injector exit. We adopted the theoretical approach of [28], and backtracked a flat distribution in energy and current from the linac end to the injector exit. Our main experimental goal was to reproduce at the injector exit the current distribution reported in [28], scaling the bunch charge from 800 pC to the actual nominal charge of 500 pC. LiTrack [35] simulations were performed to determine the optimized machine settings to linearize the LPS, starting with the ramped current profile of Fig. 3(a). We adopted the two-stage compression scheme to have a greater freedom, aiming to obtain a final peak current of ≈ 500 A. LiTrack results [Fig. 3(b)] predict an electron bunch with a final very flat energy and current profile.

The ramped current profile was obtained by exploiting the FERMI PIL system that is based on a high-energy per-pulse (15 mJ) Ti:Sapphire laser at 783-nm wavelength

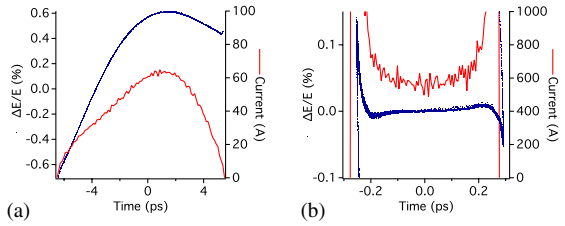

FIG. 3 (color online). LiTrack-predicted bunch current and energy profiles at the injector exit, 100 MeV (a), and at the end of the linac, 1.4 GeV (b).

which is converted to 261-nm output by a Third Harmonic Generation (THG) system. This system can produce high-quality pulses with durations ranging from 3 to 12 ps (FWHM) together with choice of different temporal shapes [36]. A ramped intensity profile was generated by adding a second THG conversion crystal appropriately positioned at a proper distance from the first. Angularly detuning this second THG crystal produces a pulse in the UV, slightly shifted in wavelength. Due to the linear chirp of the input IR pulse, this second peak is also shifted in the time domain and can be adjusted to have the appropriate temporal separation and intensity needed to obtain the desired final shape, given by the superposition of the two peaks. Ref. [37] showed that a quadratic ramp laser profile produces an electron bunch density that, due to longitudinal space charge forces in the semi-relativistic regime, evolves into a current distribution with a ramp that is linear along a large part of the bunch. Downstream of the injector ($E \approx 100$ MeV), the current profile remains nearly constant

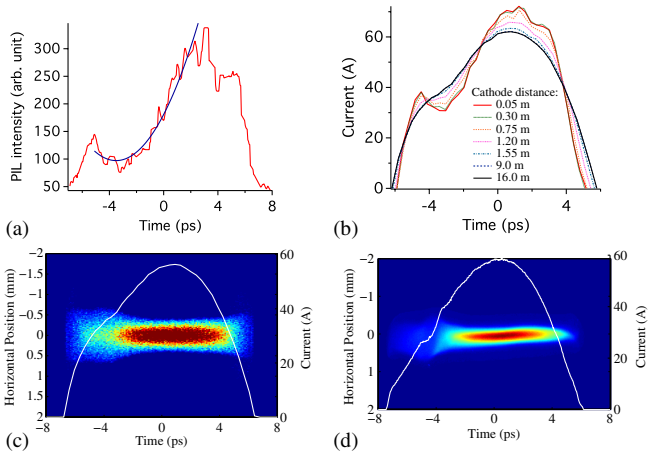

FIG. 4 (color online). Simulation and measurements of the ramped current distribution. (a) PIL temporal profile shape and quadratic polynomial fit, (b) GPT-predicted electron beam current profile evolution from the cathode to the end of the injector ($E \approx 100$ MeV), (c) top view of an uncompressed beam after BC1 ($E \approx 320$ MeV) as simulated by Elegant, (d) experimental time-resolved measurements also at 320 MeV with the post-BC1 deflector. In (c) and (d) the current profile is shown as a white line (right axis).

TABLE II. Ramped-bunch time-resolved measurements following BC1 compression to ≈ 200 A peak current, including Courant-Snyder parameters α and β. The first row refers to the projected values measured by enclosing 80% of the total bunch charge.

	ε_x (mm mrad)	β_x (m)	α_x
Projected (80%)	1.26 ± 0.13	26.4 ± 0.1	4.7 ± 0.1
Tail	1.17 ± 0.10	24.7 ± 2.0	5.0 ± 0.4
Core	1.25 ± 0.08	25.5 ± 0.7	5.8 ± 0.1
Head	1.68 ± 0.10	48.0 ± 1.7	11.3 ± 0.4

and can be directly measured with the deflecting cavity positioned after BC1, setting the chicane straight to suppress longitudinal compression. The PIL temporal shape has been iteratively manipulated starting from the profile described in [37] to obtain the desired electron bunch distribution of Fig. 3(a). Figure 4(a) shows the PIL shape as determined by a cross-correlation between the shaped UV pulse and a fraction of the laser oscillator pulse that seeds the PIL amplifier system. GPT [38] simulations of the electron longitudinal profile generated by the aforementioned quadratic PIL shape are displayed in Fig. 4(b). The resultant ramped current profile is shown in Fig. 4(d) and is in good quantitative agreement with corresponding Elegant [39] simulation predictions [Fig. 4(c)]. In future experiments we will exploit a UV temporal shaping setup based on a 4-f type system that incorporates high efficiency transmission gratings and a piezo-deformable mirror as a phase modulator. This will extend our shaping capability, allowing generation of a larger set of ramped bunches and detailed experimental study of the correlation between the PIL-shape coefficients and the final electron LPS.

The PIL spot size was increased in this ramped configuration from the nominal radius of 0.65 to 0.83 mm to limit space charge effects in the high current electron beam tail. An associated drawback to this change is a ≈ 30% increment of the beam thermal emittance [40]. Since the current density is not uniform in time, each slice has a different plasma oscillation frequency; the minimum projected emittance is then found by simultaneously optimizing the injector solenoid magnet and rf gun phase settings [41]. At the injector exit we measured a normalized projected emittance of 1.1 ± 0.1 mm mrad, while the typical value for the nominal flat-top bunch ranges from 0.65 to 0.80 mm mrad [29]. This increase is consistent with the higher expected thermal emittance at the cathode associated with the larger spot size and is also in agreement with GPT simulation results. Additional preliminary time-resolved measurements of a beam compressed by BC1 to ≈200 A (see Table II) have shown an uniform behavior along the bunch apart from the head region that is mismatched because of its lower current density. Table II also reports the projected values measured over 80% of the bunch charge. They are very close to the values measured in the core and in the tail, and are used for matching the optics in the downstream linac and in the undulator. These values are within the FERMI FEL normalized emittance requirement of 1.5 mm mrad [11].

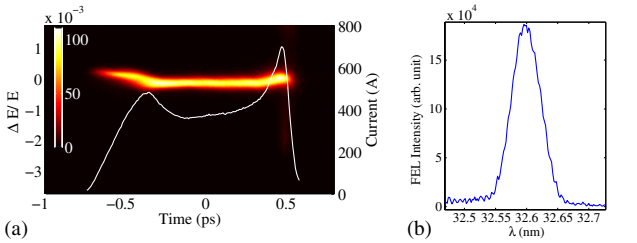

FIG. 5 (color online). (a) Electron LPS and current profile (white line, right axis) of the linearly ramped bunch profile measured at the linac end ($E \approx 1.4$ GeV), obtained in the ramped configuration. The 300 fs bunch core has a nearly constant incoherent energy spread of about 150 keV. (b) FEL spectrum at 32 nm produced with this beam.

After verifying that the beam was longitudinally shaped as desired, it was then compressed with both BC1 and BC2 to a ≈ 400–500 A peak current by using machine settings suggested by the LiTrack simulations. The resulting LPS at the linac end was then measured (Fig. 5). An almost complete compensation of the nonlinear terms has been obtained: the quadratic and cubic chirp fitting parameters $\chi_2 = 0.3$ MeV/ps^2 and $\chi_3 = 5$ MeV/ps^3 are abated by factors of 100 and 10, respectively, relative to the nominal flat-top case.

As a preliminary test, this beam was sent into FERMI's HGHG undulator line together with a 260-nm, 150-fs external seed laser pulse. We obtained coherent FEL emission at 32 nm with properties similar to those measured with nominal beam parameters [7] [see Fig. 5(b)]. This confirms that the small emittance increase associated with a ramped injector current does not seriously affect FEL performance. A detailed comparison of FEL performance with this novel beam driver versus normal operation will be the subject of future investigations.

An accompanying advantage of this linearly ramped current distribution is its similarity to the optimum current profile theoretically foreseen to linearize the CSR effects in a chicane [42]. Thus, proper longitudinal pulse shaping at the PIL could in principle linearize simultaneously both the wakes produced in rf linac structures and those associated with a bunch compressor chicane.

In conclusion, an experiment performed at FERMI validates the theoretical approach earlier presented in [28] and holds the promise of linearizing the final LPS in the presence of strong longitudinal wakefields. This result finds application not only to the high-gradient BTW sections of FERMI, but also to a number of other cases where longitudinal wakefields are dominant. Examples are the existing C-band accelerators at PSI and SACLA and future linacs based on X-band technology (e.g., the X-band

linacs described in the conceptual studies for the New Light Source [43] and compact X-ray FEL designs [44]), but also include the reduction of the wakefields generated in undulators [45].

This work was funded by the FERMI project of Elettra-Sincrotrone Trieste, partially supported by the Ministry of University and Research under Grants No. FIRB-RBAP045JF2 and No. FIRB-RBAP06AWK3.

*giuseppe.penco@elettra.eu

[1] G. A. Loew and J. W. Wang, SLAC Report No. SLAC-PUB-3598 (1985).
[2] F.-J. Decker *et al.*, SLAC Report No. SLAC-PUB-6604 (1994).
[3] M. Tigner, Nuovo Cimento **37**, 1228 (1965).
[4] P. Piot, D. R. Douglas, and G. A. Krafft, Phys. Rev. ST Accel. Beams **6**, 030702 (2003).
[5] P. Ribic and G. Margaritondo, J. Phys. D **45**, 213001 (2012).
[6] P. Emma *et al.*, Nat. Photonics **4**, 641 (2010).
[7] E. Allaria *et al.*, Nat. Photonics **6**, 699 (2012).
[8] J. Amann *et al.*, Nat. Photonics **6**, 693 (2012).
[9] L. H. Yu, Phys. Rev. A **44**, 5178 (1991).
[10] W. Fawley and G. Penn., Sincrotrone Trieste Tech. Note No. ST/F-TN-06/07; G. Penn, Sincrotrone Trieste Tech. Note No. ST/F-TN-06/12 (2006).
[11] C. J. Bocchetta, *et al.*, FERMI@Elettra CDR, http://www.elettra.trieste.it/FERMI, (2007).
[12] A. A. Lutman, G. Penco, P. Craievich, and J.Wu, J. Phys. A **42**, 045202 (2009).
[13] A. A. Lutman, G. Penco, P. Craievich, and J.Wu, J. Phys. A **42**, 085405 (2009).
[14] A. Marinelli, C. Pellegrini, L. Giannessi, and S. Reiche, Phys. Rev. ST Accel. Beams **13**, 070701 (2010).
[15] B. Jia, Y. K. Wu, J. J. Bisognano, A. W. Chao, and J. Wu, Phys. Rev. ST Accel. Beams **13**, 060701 (2010).
[16] E. Allaria *et al.*, in Proceedings of the Free-Electron Laser Conference, TUOB02, Nara, Japan, 2012 edited by T. Tanaka and V. R. W. Schaa.
[17] R. J. England, J. Rosenzweig, G. Andonian, P. Musumeci, G. Travish, and R. Yoder, Phys. Rev. ST Accel. Beams **8**, 012801 (2005).
[18] P. Emma, SLAC Report No. LCLS-TN-01-1, November 2001.
[19] K. Flöttmann *et al.*, DESY Report No. DESY-TESLA-FEL-2001-06 (2001).
[20] K. Bane, SLAC Report No. SLAC-PUB-11829, (2006).
[21] A. Chao, *Physics of Collective Beam Instabilities in High Energy Accelerators* (Wiley, New York, 1993).
[22] P. Craievich, T. Weiland, and I. Zagorodnov, Nucl. Instrum. Methods Phys. Res., Sect. A **558**, 58 (2006).
[23] CLIC Conceptual Design Report, CERN Report No. CERN-2012-007, Geneva 2012.
[24] R. Ganter*et al.*, Swiss FEL Conceptual Design Report, PSI Bericht Nr. 10-04, April 2012.
[25] I. Ishikawa *et al.*, Nat. Photonics **6**, 540 (2012).
[26] E. L. Saldin, E. A. Schneidmiller, and M. V. Yurkov, Nucl. Instrum. Methods Phys. Res., Sect. A **398**, 373 (1997).
[27] Z. Huang, M. Borland, P. Emma, J. Wu, C. Limborg, G. Stupakov, and J. Welch, Phys. Rev. ST Accel. Beams **7**, 074401 (2004).
[28] M. Cornacchia, S. Di Mitri, G. Penco, and A. A. Zholents, Phys. Rev. ST Accel. Beams **9**, 120701 (2006).
[29] G. Penco *et al.*, JINST **8**, P05015 (2013).
[30] S. Di Mitri *et al.*, Nucl. Instrum. Methods Phys. Res., Sect. A **608**, 19 (2009).
[31] G. Penco *et al.*, in Proceedings of the 34th International Free-Electron Laser Conference, WEPD20, Nara, Japan, 2012 edited by T. Tanaka and V. R. W. Schaa.
[32] M. Venturini, Phys. Rev. ST Accel. Beams **10**, 104401 (2007).
[33] S. Di Mitri *et al.*, in Proceedings of the 32th International Free-Electron Laser Conference, THPB03, Malmö, Sweden, 2010 edited by N. Cutic, L. Liljeby, A. Meseck, A. Nyberg, V. Schaa, S. Thorin, and S. Werin.
[34] S. Spampinati *et al.*, in Proceedings of the 35th International Free-Electron Laser Conference, WEPS067, Manhattan, NY, USA, 2013 edited by T. Tanaka and V. R. W. Schaa.
[35] K. Bane and P. Emma, SLAC-PUB-11035 (2005).
[36] M. Danailov *et al.*, in Proceedings of the 29th International Free-Electron Laser Conference, WEPPH014, Budker INP, Novosibirsk, Russia, 2007 edited by B. Goldenberg, V. Eliseev, A. Zhirkova, P. Budz.
[37] G. Penco *et al.*, in Proceedings of the 28th International Free-Electron Laser Conference, THPPH027, Berlin, Germany, 2006 edited by V. R. W. Schaa.
[38] General Particle Tracking Code, Pulsar Physics, http://www.pulsar.nl/gpt/index.html.
[39] M. Borland, Argonne Report No. APS LS-287, 2000).
[40] D. H. Dowell and J. F. Schmerge, Phys. Rev. ST Accel. Beams, **12**, 074201 (2009).
[41] L. Serafini, J. B. Rosenzweig, Phys. Rev. E **55**, 7565 (1997).
[42] C. Mitchell, J. Qiang, and P. Emma, Phys. Rev. ST Accel. Beams, **16**, 060703 (2013).
[43] R. Bartolini, Nucl. Instrum. Methods Phys. Res., Sect. A **657**, 177 (2011).
[44] Y. Sun, C. Adolphsen, C. Limborg-Deprey, T. Raubenheimer, and J. Wu, Phys. Rev. ST Accel. Beams **15**, 030703 (2012).
[45] J. Qiang and C. E. Mitchell, Proceeding of the 35th International Free-Electron Laser Conference, MOPS065, Manhattan, NY, USA (2013).